UNITED NATIONS UNIVERSITY
UNU-GTP
Geothermal Training Programme

Orkustofnun, Grensasvegur 9,
IS-108 Reykjavik, Iceland

Reports 2014
Number 34

FLUID-ROCK INTERACTION AND INITIAL AQUIFER GEOCHEMISTRY IN THE OLKARIA GEOTHERMAL SYSTEM

Edwin Wafula Wanyonyi
Kenya Electricity Generating Company Ltd. - KenGen
P.O. Box 785-20117, Naivasha
KENYA
ewwafula@kengen.co.ke

ABSTRACT

The Olkaria geothermal field is one of the quaternary volcanic centres in the Kenyan Rift valley. Geochemical methods have been applied in studying the elemental origin and reactions at depth. Fluid-rock interaction is one of the key reactions of interest in geothermal systems. Two models have been postulated in the evaluation of aquifer fluid composition. The first model assumes a single-phase liquid aquifer, while in the second model one assumes a two-phase fluid aquifer: vapour and liquid. The concentration of non-volatile components is unaffected by the choice of model except for fluid discharges approaching dry vapour. However, the concentration of volatiles is greatly influenced by the selection of a model for calculating aquifer fluid composition. As a consequence, solute geothermometers like quartz and Na/K have similar temperatures for the two models, whereas gas geothermometers like H_2S show distinctively lower values when assuming two-phase aquifers. Many common minerals observed within the Olkaria geothermal system are observed to be saturated, including calcite, fluorite, epidote-clinozoisite, prehnite, feldspars and pyrite. Based on this, the mineral-fluid equilibrium is considered to control the fluid chemical composition. Mineral buffer reactions are considered to control the H_2S and H_2 volatile concentrations, whereas the concentration of CO_2 may either or both be controlled by mineral equilibria in the geothermal system or by an external source.

1. INTRODUCTION

Geochemistry is one of the major disciplines that have been applied in the exploration and development of geothermal systems. The primary goal of geochemical study of geothermal fluids is to trace their elemental origin and reactions. The latter makes the basis for estimating subsurface temperatures based on the chemical composition of samples collected at the surface. Among the key reactions of interest in geothermal systems is fluid-rock interaction. Previous studies have demonstrated a close approach to equilibrium between common geothermal minerals and the fluids within the reservoir, hence controlling the composition of most major elements in the fluid (Giggenbach, 1981; Arnórsson et al., 1983). However, the assessment of fluid-rock equilibria from the fluid composition of surface well discharges largely relies on the assumptions made when calculating the subsurface aquifer fluid composition. In the case of two-phase well discharges that have measured enthalpies closely corresponding to liquid-only aquifers and the aquifer temperatures, the assumption of adiabatic boiling upon ascent is considered valid. On the other hand, many well discharges have excess enthalpy

characteristics, i.e. a high vapour-to-liquid water ratio relative to a liquid-only aquifer and the aquifer temperatures. In this case, the cause of the excess enthalpy has to be taken into consideration when assessing the aquifer fluid composition. The reasons for such an excess enthalpy character may be many, including vapour formation in the aquifer due to heat induced boiling and the formation of aquifer vapour. Alternatively, depressurization boiling may lead to separation of vapour and liquid water, either fully or partially, the latter referred to as phase segregation. In recent years, phase segregation has been concluded to be the cause of excess enthalpy in many cases, whereas heat induced boiling is less well documented (Arnórsson et al., 2007; Karingithi et al., 2010; Scott et al., 2014). This project aims to assess the aquifer conditions and fluid-rock interaction based on two different models. Model 1 is based on a calculated enthalpy and considers a single-phase liquid only reservoir, while model 2 considers a two-phase liquid and vapour reservoir. Model 2 is based on a measured enthalpy and considers the presence of excess enthalpy in the system. In the evaluation of the initial aquifer composition, both models are postulated and the results are compared. The component concentrations for volatile and non-volatile species are considered in characterising the initial aquifer conditions from the two models. Geothermometer temperatures are also determined considering these aquifer concentrations and a comparison is done with the measured reservoir temperatures. Then it will be possible to determine what the contributing process to the excess enthalpy in the wells could be. The mineral saturation state is dependent on the aquifer composition of the fluid. Thus, the mineral saturation state for selected minerals: andradite, grossular, calcite, clinozoisite, epidote, fluorite, magnetite, prehnite, pyrite, pyrrhotite and wollastonite, are modelled.

2. OLKARIA GEOTHERMAL SYSTEM

2.1 Study area

The Olkaria geothermal project is located approximately 120 km northwest of Nairobi, on the floor of the southern segment of Kenya's Rift Valley. The Olkaria concession covers an area of 204 km^2. About 14 prospects have been identified in the Kenyan Rift Valley as having a potential for geothermal development. Of these, geothermal exploration has been done in almost all these areas, but currently development is limited to Olkaria, Eburru and Menengai Geothermal fields. Currently, 217 wells have been drilled in Olkaria, both vertical and directional wells, including reinjection, monitoring and production wells. The Olkaria geothermal field is divided into seven sectors: Olkaria E, Olkaria NE, Olkaria C, Olkaria SW, Olkaria NW and Olkaria SE (Figure 1). Production from geothermal resources started in 1981 with the construction of the OlkariaI power plant that currently has a production capacity of 45 MW. An additional 140 MW power plant is under construction in this part of the field. In the Olkaria NE, the Olkaria II power plant exists with a production capacity of 105 MW. An additional power plant is under construction that will add a further 140 MW to the grid in the Olkaria domes area.

2.2 Geology

According to Strecker et al. (1990), the Olkaria volcanic complex is part of the volcanic centres in the Central Kenya Rift, associated with quaternary silicic volcanism. These include the Suswa, Longonot, Eburru and Menengai volcanic centres. The Olkaria geology has been divided into five broad litho-stratigraphic groups based on the age of the stratigraphy and lithology. These include the Mau tuffs, Plateau trachytes, Olkaria basalts and upper Olkaria volcanics (I only count 4, not 5.). The rocks occurring on the surface in the Olkaria geothermal area include rhyolite flows and pyroclastic deposits. Lacustrine deposits crop out in isolated occurrences within Olkaria but are abundant closer to Lake Naivasha. The distal deposits have been associated with previous high stands of Lake Naivasha (Naylor, 1972). The latest ash-fall deposits that blanket most lava flows in Olkaria originated mainly from Longonot volcano and, to a smaller extent, from Suswa volcano (Odongo, 1984). The youngest volcanic activity at Olkaria occurred about 250 years ago and produced the Ololbutot lava flow, which is an

FIGURE 1: Map of the Greater Olkaria volcanic complex showing major structures (from Clarke et al., 1990)

important landmark in the area (Clarke et al., 1990). The Mau formation is the geothermal reservoir rock for the western sector. In the eastern Olkaria geothermal field, there occurs a basaltic formation at between 1000-1500 m above sea level. The formation is considered a cap-rock (aquitard) to the geothermal system and temperatures rise sharply below it. The formation is absent in the west field. Overlying the basalt formation is the upper rhyolite unit that extends from the east to the western fields.

The fault system in Olkaria is dominated by a N-S pattern. Other common trends are NW and ENE. A ring structure defined by lava domes occurs in the eastern Olkaria area and marks the eastern and southern boundary of the Domes field. Sheets of recent and quaternary lavas, pyroclastics and lacustrine sediments blanket most of the faults in the area. The N-S faults are active and open since the dominant tectonic regime within the central rift is extensional with a minimum stress field oriented in a general WNW-ESE direction (Strecker et al., 1990).

Hydrothermal mineral characterisation is one of the important parameters in the classification of geothermal systems. Kandie et al. (2014) described the hydrothermal minerals of the Olkaria system as analysed from well cuttings. The alteration minerals have been defined by the occurrence of certain specific index minerals and clay minerals. These are: smectite-zeolite zone (0-300), mixed Layer Clay (smectite-chlorite-illite zone), chlorite-illite zone (300-550 m), epidote-chlorite-illite zone (550-1400 m) and actinolite-epidote chlorite-illite zone (1400-3000 m). Lagat (2004) classified the hydrothermal mineralogy of the Olkaria geothermal system. The main minerals identified are: albite, actinolite, biotite, calcite, chlorite, chalcedony, epidote, fluorite, garnet, illite, adularia, pyrite and quartz.

2.3 Geochemistry

The Olkaria geothermal field has varied chemistry in the different sectors within it. The water discharged from wells in the Olkaria field is low in dissolved solids, compared to water from most other drilled high-temperature geothermal fields in the world, with chloride concentrations in the water at the weir box ranging between 50 and 1100 ppm. The water from wells in Olkaria East and Northeast are the highest in chloride. The high chloride could be a result of up-flow of deep high-temperature geothermal fluid, although progressive boiling by heat flow from the rock may also be a contributing factor, as in the Olkaria East field. A study by Wambugu (1995) established that in Olkaria West field the chloride concentrations are quite low, except in well OW-305, which discharges water similar to that discharged from the wells in the Olkaria East and Olkaria Northeast fields. Well OW-305 is thought to be tapping the up-flow fluid in the Olkaria West field. The well discharges in Olkaria West are distinctly highest in carbon dioxide. The CO_2 source is considered to be predominantly from the magma heat source of the geothermal system, although carbon present in the rock may contribute as much. The chloride, sulphate and bicarbonate ternary plots show that wells in the Olkaria East production field and in Olkaria Northeast discharge sodium-chloride type water, while the Olkaria West has a bicarbonate water type. Wells in the Olkaria Central and Domes fields discharge a mixture of chloride and bicarbonate water. Temperature and pressure distributions across the entire field have been studied and indicate that fluid movement in the Olkaria geothermal area is associated with tectonic structures. The Olkaria East reservoir is two-phase, at least to the depth penetrated by the deepest wells. High temperatures are observed in Olkaria West, Olkaria Northeast and Olkaria Domes, while lower ones are observed in Olkaria Central. The ENE-WSW trending Olkaria fault zone is the most important permeable structure in the entire Olkaria geothermal area. The geothermal reservoir in the north (including Olkaria Domes) is liquid-dominated and has no steam cap, whereas south of the fault the reservoir is a liquid-dominated two-phase system overlain by a steam-dominated zone (Ambusso and Ouma, 1991). The Olkaria reservoir has a shallow two-phase steam-dominated zone at 240-250°C, and a deeper zone that is liquid-phase at up to 340°C. Mixing of this liquid in lower shallower zones results in high total enthalpy conditions in some wells, causing excess enthalpy in the well discharge by excess boiling. Enthalpy chloride diagrams from the well indicate a deep upwelling of a fluid at 320°C to 340°C, cooling to 280°C before the onset of boiling and mixing in the NE production field and E production field sectors. Enthalpy-chloride models for the domes area suggest that deeper temperatures are closer to 330°C and that reservoir boiling seems to start at this temperature without prior cooling. Na/K ratios have been used to locate major up-flow zones in geothermal fields (Arnórsson and D'Amore, 2000) with the lowest ratios being closest to up-flow zones. The Na/K geothermometer is based on this ratio with high temperatures obtained at lower ratios. Na/K temperatures for the Olkaria field sectors show good agreement with measured temperatures at 0 m above sea level. The temperatures, together with the chloride distribution in the field, delineate zones of up-flow in the geothermal area. The Na/K temperature shows distinct up-flow zones in each of the three sectors of the Olkaria field, but delineates a subtle one for Olkaria west around wells OW-301 and OW-308.

3. DATA BASE AND DATA HANDLING

The principle method used in the acquisition of geochemical data is sampling and analysis of well discharges. The data used in this study is from 24 wells in the Olkaria geothermal system, with 15 of these wells representing wells that are currently under production. The data is referred to from the analysis by Karingithi, et al. (2010)

3.1 Sampling and analysis

Sampling and collection of fluids for chemical analysis were based on the procedures described by Arnórsson et al. (2007) for high temperature wells. These wells discharge a two-phase fluid and

sampling and collection of samples was done on the two-phase line. The liquid and steam samples were collected using a webre separator. Fluid was allowed to flow into the separator by opening the vents. The valves in the separator were adjusted so that the pressure in the webre separator was close to that in the well head. The sampling pressure and temperature were recorded. For the liquid sample, the needle valve and the ball valve of the webre separator were completely opened to release steam and to ensure that only liquid was sampled from the water port (no bubbles), collected into different bottles. A micrometre filter paper was used in the filtration of the liquid samples to remove the colloidal particles. A 250 ml filtered sample acidified with 1 ml nitric acid was collected for analysis of major cations. A 10 ml sample, diluted with 90 ml deionized water, for silica analysis was collected to slow down the polymerisation of the monomeric silica in solution. A 100 ml filtered sample was precipitated with 2 ml zinc acetate for sulphate analysis. A 250 ml filtered sample was collected for analysis of boron, chloride and total solids. A 500 ml untreated sample for analysis of pH, Carbonate and conductivity was collected in a tightly corked glass bottle to avoid contamination with air. Hydrogen sulphide was titrated on site. The steam sample was collected by fully opening the water valves completely and adjusting the needle and ball valves of the separator until a dry steam was obtained. The steam was collected to an evacuated double port bottle containing 50 ml of 40% NaOH, using tubings from the separator port. The CO_2 and H_2S dissolve in the caustic solution; the other gases collect in the free space in the bulb.

The analysis was done according to standard methods for geothermal fluid analysis, as described by Ármansson and Ólafsson (2000). Analysis for H_2S in the liquid sample was done in the field by titration, using 0.001 M $HgAc_2$ with a dithizone indicator. 5 ml of NaOH was put in a 50 ml volumetric flask and filled with the sample. 0.1-5 ml was put in an Erlenmeyer flask and 5 ml acetone was added and the volume was brought up to 10 ml with distilled, deionized water. Silica analysis samples were diluted to slow the polymerization of silica. The method used for silica analysis is spectrophotometric, using the absorbance of the yellow β-molybdosilicic acid complex at a wavelength of 410 nm. The fluoride concentrations were determined with an ion selective electrode with standards prepared from NaF. The working standards were prepared from a 1000 ppm stock solution with working ranges of 5-500ppm and 0.5-50 ppm. The chloride analysis was done by argentometric titration with Silver Nitrate, using potassium chromate as an indicator. The sample was titrated with 0.1 $AgNO_3$, where the end point is the appearance of the first permanent orange colour.

3.2 Charge balance

Geochemical interpretation is based on data sampled and analysed from well discharges. This data, however, needs to meet certain criteria before credible information on the well chemistry is certain. Ways have, therefore, been devised to ensure that good data is used in the geochemical interpretation.

The first of these is the ionic balance check. Normally, it is expected that the geothermal fluids are close to neutral solutions and, hence, the negative charge and the positive should be close to null. A mathematical expression called the charge balance error has been devised to set limits within which to consider a chemical analysis as acceptable. The charge balance error can be determined based on Equation 1, although the program WATCH version 2.4 (Bjarnason, 2010) was run to accurately determine the ionic balance, given that it considers the speciation of the compounds. From the program, a balance of +/- 15 percent is considerable and the data can be used.

$$CBE\ \% = \left(\frac{\sum Z_{cat}M_{cat} - \sum Z_{an}M_{an}}{\sum Z_{cat}M_{cat} - \sum Z_{an}\,M_{an}}\right).100\% \quad (1)$$

where Z_{cat} is the charge of a given cation, M_{cat} is the molal concentration of the respective cation, Z_{an} is a charge of a given anion and $M_{an}$is the molal concentration of the respective anion.

The pH of a fluid is an important parameter, in that the mineral solubility depends on it. The pH, on the other hand, varies with the temperature of the fluid. The practise is to measure the pH at the sample site and record the temperature. On some instances, however, the pH is taken in a laboratory away from the sampling site. In such a case, the recorded pH may not represent the accurate pH of the fluid. This is because in high temperature systems, the sample would already have polymerised silica. The removal of monomeric silica in the solution increases the pH of the solution (Karingithi et al., 2010). If such is the case, then a pH correction has to be calculated on the WATCH program, especially for fluids with pH above 9.

3.3 Aquifer fluid composition

Geochemical interpretations are based on samples that are collected from well discharges at the surface. To understand the fluid-rock interactions at depth, however, the chemical composition of the fluid at aquifer conditions has to be calculated. The approach chosen here is to calculate the aquifer fluid composition involved either by assuming liquid only in the reservoir and no excess enthalpy, or alternatively assuming two-phase vapour and a liquid reservoir (Table 1).

For the models, conservation of mass and energy is assumed, i.e.

$$m_i^t = m_i^v X + m_i^{lq}(1 - X) \tag{2}$$

where $\boldsymbol{m_i^t}$ is the total concentration of the i-th component, and $\boldsymbol{m_i^v}$ and $\boldsymbol{m_i^{lq}}$ is are the concentration in the vapour and liquid phase of the same component, respectively.

For the enthalpy of the system, we have:

$$h^t = h^v X^v + h^{lq}(1 - X) \tag{3}$$

where $\boldsymbol{h_i^t}$ is the total enthalpy of the system, $\boldsymbol{h^v}$ and $\boldsymbol{h^{lq}}$ are the enthalpies of the vapour and liquid phases, respectively, and X is the steam fraction given by:

$$X = \frac{h^t - h^{l,q}}{h^v + h^{l,q}} \tag{4}$$

The WATCH program version 2.4 (Bjarnason, 2010) was used to calculate the aquifer fluid composition from the data on the well discharge composition. In the case of a liquid-only reservoir, the reservoir enthalpy of the system was calculated assuming liquid-only water to be present at reservoir temperatures. In the case of a two-phase vapour and liquid water reservoir, the measured discharge enthalpy was included to solve the formulas of mass and enthalpy. The former approach is termed Model 1 here, and the second approach is Model 2.

3.4 Geothermometry

Chemical geothermometers have been applied in the estimation of reservoir temperatures. These include both the solute geothermometer and gas geothermometer. The three geothermometers included here were silica, Na/K and H_2S.

The silica geothermometer is based on quartz solubility at >180˚C, according to the chemical reaction:

$$\text{quartz} + 2\text{H}_2\text{O} = \text{H}_4\text{SiO}_4 \tag{5}$$

The quartz solubility constant, as well as the silica geothermometer temperatures, are based on Gunnarsson and Arnórsson (2000) to give:

$$t_{qtz} = -54.8 + 0.3729.X - 5.602 \times 10^{-4}.X^2 + 5.719.10^{-7}.X^3 + 73.917.logX \tag{6}$$

where X is the SiO_2 concentration in ppm.

TABLE 1: Chemical analysis of water and steam wells in Olkaria; component concentration for water samples are in mg/kg, and mmole/kg for steam

Well	GSP	WHP	Enth. (Kj/Kg)	Aquifer T	pH	B	SO_4	Cl	CO_2	F	H_2S	SiO_2	Ca	Li	Na	K	Mg	Fe	Al	CO_2	H_2S	CH_4	H_2	N_2
					Water sample															Steam sample				
2	4.8	5.8	1839	251	9.07	6.8	28	764	74	69	1.02	643	0.73	0.5	557	92	0.010	0.020	0.660	101.1	5.61	0.722	2.94	1.94
5	4.8	5.5	2599	240	8.75	8.7	70	933	73	71	1.19	624	1.08	1.3	668	102	0.010	0.030	1.110	101	5.61	0.111	2.33	2.28
10	4.8	6	2531	261	8.57	12.9	61	1190	78	76	0.17	773	2.46	1.2	805	144	0.050	0.050	0.830	70.5	4.33	1.433	1	5
11	5	5.1	1894	246	8.94	5.7	21	696	69	64	0.34	597	0.58	1.1	497	81	0.000	0.020	0.700	53.3	9.27	0.611	2.61	1.72
15	4.5	5	2140	242	9.43	5.9	54	658	92	57	9.86	576	0.56	1.1	526	83	0.010	0.020	0.790	55	5.44	0.444	3.55	2.83
16	4.8	5	1534	228	9.37	4.9	44	586	97	64	7.14	502	0.35	1.2	503	67	0.030	0.010	0.490	68.3	4.83	0.278	4.27	6.16
19	5.2	5.5	1871	229	9.51	4.6	57	392	126	70	22.1	548	0.49	1.073	425	54	0.040	0.020	0.910	58.8	5.77	0.389	3.72	5.44
20	5.4	5.5	2541	255	8.98	14.3	22	822	110	95	1.19	778	0.92	1.789	610	97	0.050	0.380	0.430	101	9.33	0.333	4	1.28
23	5	6.1	2191	242	9.44	4	42	221	132	75	7.88	653	0.9	0.813	370	52	0.050	0.040	0.710	81	7.27	0.167	5.27	2.5
26	7.2	7.5	1881	247	9.39	2.2	24	309	104	68	13.6	657	0.24	1	336	51	0.040	0.250	0.930	129.3	9.21	0.222	4.22	3.33
28	2.1	8.1	2446	234	9.27	6.2	104	478	72	50	4.59	625	1.33	1.2	441	61	0.010	0.120	0.860	41.6	4.88	0.056	2.33	2
29	2.1	8.5	2158	241	8.87	10.1	30	509	82	84	3.91	609	0.75	1.2	417	63	0.030	0.060	0.670	45	6.66	0.056	3.77	3.33
30	2.1	8	2196	256	8.6	3.9	50	527	48	52	1.03	768	0.27	1.234	406	71	0.030	0.910	1.600	55	6.61	0	0.39	2.55
202	1.5	5.2	1104	225	9.3	2.5	75	354	1246	53	2.38	320	0.79	0.98	743	128	0.040	0.020	0.860	155.4	0.56	0.278	0	0.89
301	1.5	7.4	1653	262	8.67	6.8	112	240	2465	105	3.96	855	0.66	0.887	1283	208	0.070	0.020	0.670	4260.1	3.55	0.833	1.05	11.27
302	1.8	5.7	1234	256	9.72	3.5	54	505	578	77	3.43	744	1.04	1.5	633	101	0.080	0.020	0.780	367.5	1.11	0.389	0.33	3.22
304	2.6	3.9	1672	190	8.13	3.3	93	52	1752	24	0.97	364	3.48	1.331	959	74	1.730	0.140	0.520	11462	2.66	1.721	0.94	17.37
306	1.8	4	1037	224	9.15	6.3	50	251	1081	62	2.9	551	1.2	1.2	850	96	0.080	0.090	1.380	1136.8	2.89	0.944	0.56	7.83
709	1.9	7.1	1921	276	9.93	5.1	73	770	318	28	6.54	649	1.41	1.8	846	218	0.040	0.020	0.890	56.1	1.44	0.278	1.89	3.05
714	2.8	14.9	1303	267	9.54	3.6	35	682	135	66	8.44	739	0.88	1.4	557	108	0.060	0.010	1.050	81	4.38	0.333	1.22	3.39
719	2.9	8	1259	241	9.38	4.8	83	544	162	46	4.46	588	1.09	1.15	536	81	0.040	0.020	1.510	155.4	5.33	0.444	1.05	4.11
901	1.6	4.3	1854	220	9.8	2.4	124	280	566	80	18.3	529	0.72	2.6	506	57	0.030	0.030	0.680	186.5	4.94	0.333	2.44	5.16
902	1	3.2	1108	209	9.55	1.5	100	212	434	52	2	477	1.31	1.3	448	41	0.050	0.080	2.120	178.7	0.5	0.777	0.06	13.54
903	1.3	4	953	206	9.43	1.1	103	178	634	46	3.51	443	0.71	1.8	493	47	0.040	0.020	1.220	278.1	1.05	0.722	0.22	18.98

GSP = sampling pressure (bar g); WHP = well head pressure (bar g); Enth = enthalpy (kJ/kg); T = temperature (°C)

The Na/K geothermometer is based on the equilibrium between low-albite and microcline, according to the chemical reaction:

$$low - albite + K^+ = microcline + Na^+ \quad (7)$$

The temperature function based on the solubility of low-albite and microcline is given by Arnórsson and Stefansson (1999):

$$t_{Na/K} = 733.6 - 770.551.Y + 378.189.Y^2 - 95.753Y^3 + 9.544.Y^4 \quad (8)$$

where Y is the logarithm of the Na^+/K^+ activity ratio.

The H_2S geothermometer temperatures were calculated based on the chemical reaction:

$$\frac{1}{4}\mathrm{pyr} + \frac{1}{2}\mathrm{pyrr} + \mathrm{H_2O_l} = \frac{1}{4}\mathrm{mag} + \mathrm{H_2S_{aq}} \quad (9)$$

using the proposed equation given by Karingithi et al. (2010):

$$t_{H_2S} = 252.7 + 65.573.Z + 5.063.Z^2 + 0.1641.Z^3 \quad (10)$$

where Z is the concentration of H_2S in the aquifer water in mmoles/kg.

3.5 Mineral saturation

The mineral saturation state is calculated, based on:

$$SI = \log(Q/K) \quad (11)$$

where K is the equilibrium solubility constant and Q is the activity product (Q) given by:

$$Q = \prod_i a_i^{v_i} \quad (12)$$

and a_i is the respective aqueous specie's activities raised to the power of its stoichiometric coefficient, v_i, which is negative for reactants and positive for products. Here, the aqueous speciation was calculated using the WATCH 2.4 program (Arnórsson et al., 1982; Bjarnason, 2010). The solubility constants for the pure minerals and mineral buffer reactions were taken from Karingithi et al. (2010). All minerals were taken to be pure, i.e. their activities were assumed to be unified. The minerals considered in this study, together with their equilibrium constant temperature functions, are given in Tables 2 and 3.

4. AQUIFER FLUID COMPOSITION

The aquifer fluid composition was assessed with the aid of the WATCH program (Arnórsson et al., 1982; Bjarnason, 2010) version 2.4. The program uses the chemical composition of vapour and water collected at the surface from well discharges. Two approaches were used to calculate the aquifer fluid composition; Model 1 assumes a liquid-only aquifer, and Model 2 assumes a two-phase aquifer of vapour and water. The results and the aquifer fluid composition of the two models are shown in Tables 4 and 5.

The concentrations of non-volatile elements for the two models are similar, except for the discharge fluids that approach that of pure steam. Yet, the concentrations of non-volatiles in the liquid phase of two-phase reservoirs are somewhat lower in most cases. Non-volatile elements include, for example, SiO_2, Na, K, Ca, Mg, Cl, F, SO_4, Al and Fe. With respect to volatiles like CO_2, H_2S, H_2, and CH_4, a marked difference was observed between the two models. The reason for this is the volatiles portioning into the vapour phase, some completely upon initial boiling like H_2 and CH_4, whereas others are distributed between the two phases, like CO_2 and H_2S. As a result, the aqueous concentration of the

non-volatiles is low when assuming two-phase reservoirs, compared to single-phase liquid reservoirs. Also, as the CO_2 and H_2S are among the major acids buffering the aquifer water pH, the assumption of liquid-only reservoirs results in lower pH values, the difference being ~0.5 on the pH scale.

TABLE 2: Temperature equations for equilibrium constants and corresponding mineral dissolution reactions; they are valid in the range 0-350°C at P_{sat}

	Reaction	LogK(T)
1	$and + 8H_2O = 3Ca^{+2} + 2Fe(OH)_4^- + 3H_4SiO_4^0$	+940.225-154193.3/T+0.58092.T-0.0002971.T^2- 421.727logT
2	$cal + 2H^+ = Ca^{+2} + H_2O + CO_{2aq}$	-68.271+4385.24/T-0.007525.T+25.856logT
3	$czo + 12H_2O_l = 2Ca^{+2} + 3Al(OH)_4^- + 3H_4SiO_4^0 + OH^-$	+36.052-6854.78/T+0.13236.T-0.00013749.T^2-33.508logT
4	$epi + 12H_2O_l = 2Ca^{+2} + Fe(OH)_4^- + 3Al(OH)_4^- + 3H_4SiO_4^0 + OH^-$	+893.547-27077.4/T+0.54124.T-0.0003022.T^2-398.380logT
5	$flu = Ca^{+2} + 2F^-$	+66.54-4318/T-25.47logT
6	$gro + 4H^+ + 8H_2O_l = 3Ca^{+2} + 2Al(OH)_4^- + 3H_4SiO_4^0$	-517.662+17623.7/T-0.14343.T+203.808logT
7	$mag + 4H_2O_l = 2Fe(OH)_4^- + Fe^{+2}$	+949.951-24258.2/T+0.51474.T-0.0002402.T^2-417.136logT
8	$pre + 10H_2O_l = 2Ca^{+2} + 2Al(OH)_4^- + 3H_4SiO_4^0 + 2OH^-$	+833.950-25642.8/T+0.5035.T-0.0002941.T^2-369.297logT
9	$pyr + 2H^+ + H_{2aq} = 2H_2S_{aq} + Fe^{+2}$	-3.043+1579.06/T+0.001987.T+0.120logT
10	$pyrr + 2H^+ = H_2S_{aq} + Fe^{+2}$	-3.043+1579.06/T+0.001987.T+0.120logT
11	$qtz + 2H_2O_l = H_4SiO_4^0$	-34.188+197.47/T-5.851.10^{-6}.T^2+12.245logT
12	$wol + 2H^+ + H_2O_l = Ca^{+2} + H_4SiO_4^0$	-127.096+8151.38/T-0.02981/T-0.02981.T+49.282logT

The source for the thermodynamic data used to derive these equations is given in chapter 3 of the text. Also referred to from Karingithi et al., (2010). Unit activity has been taken for minerals and water. The minerals considered are: and: andradite, cal: calcite, czo : clinozoisite, epi : epidote, flu : fluorite, gro : grossular, mag : magnetite, pre : prehnite, pyr : pyrite, qtz : quartz, wol : wollastonite.

TABLE 3: Temperature equations for the equilibrium constants for mineral pairs that control gas concentrations in solution; the equations are valid in the range 0-350°C at P_{sat}

Species	Reaction	LogK(T)
CO_2	$czo + cal + \frac{3}{2}qtz + H_2O = \frac{3}{2}pre + CO_{2aq}$	- 0.890+7251/T^2-1710.6/T+0.004188T+0.0000002683T^2-0.0641logT
CO_2	$\frac{2}{5}czo + cal + \frac{3}{5}qtz = \frac{3}{5}gro + \frac{1}{5}H_2O_l + CO_{2aq}$	-1.449-40536/T^2-2135.9/T+0.0065639T+0.0000002725T2-0.193logT
H_2S	$\frac{1}{3}pyr + \frac{1}{3}pyrr + \frac{2}{3}pre + \frac{2}{3}H_2O_l = \frac{2}{3}epi + H_2S_{aq}$	13.608+592324/T2-9346.7/T-0.043552T+0.0000291647T2+5.139logT
H_2S	$\frac{2}{3}gro + \frac{1}{3}pyr + \frac{1}{3}pyrr + \frac{2}{3}qtz + \frac{4}{3}H_2O_l = \frac{2}{3}epi + \frac{2}{3}wol + H_2S_{aq}$	13.659+555082/T^2-9256.6/T-0.043608T+0.0000286137T^2+5.148logT
H_2S	$2gro + \frac{1}{4}pyr + \frac{1}{2}mag + 2qtz + 2H_2O = 2epi + 2wol + H_2S_{aq}$	-0.836-216659/T^2-2847.3/T+0.008524T-0.0000023667T^2+0.152logT
H_2S	$\frac{1}{4}pyr + \frac{1}{2}pyrr + H_2O_l = \frac{1}{4}mag + H_2S_{aq}$	13.589+590215/T^2-9024.5/T-0.044882T+0.0000029780T^2+5.068logT
H_2	$\frac{4}{3}pyrr + \frac{2}{3}pre + \frac{2}{3}H_2O_l = \frac{2}{3}epi + \frac{2}{3}pyrr + H_{2aq}$	-1.640-124524/T^2-777.19/T-0.0005501T+0.0000007756T^2-0.565logT
H_2	$\frac{2}{3}gro + \frac{4}{3}pyrr + \frac{2}{3}qtz + \frac{4}{3}H_2O_l = \frac{2}{3}epi + \frac{2}{3w}wol + \frac{2}{3}pyr + H_{2aq}$	-1.544-151109/T^2-752.389/T-0.0005868T+0.0000070080T^2-0.532logT
H_2	$6gro + 2mag + 6qtz + 4H_2O_l = 6epi + 6wol + H_{2aq}$	1.444-273812/T^2-3962.1/T+0.002401T+0.0000013047T^2-0.979logT
H_2	$\frac{2}{3}pyr + H_2O_l = \frac{3}{4}pyr + \frac{1}{4}mag + H_{2aq}$	-1.654-95456.8/T^2-621.84/T-0.001257T+0.0000075697T^2-0.600logT

The source of the thermodynamic data is as described in Table 2.

TABLE 4: Aquifer fluid composition based on a two-phase liquid and vapour reservoir (Model 2); concentrations are in mg/kg Output from the program WATCH (Bjarnason, 2010)

Well	pH	B	SO_4	Cl	CO_2	F	H_2S	SiO_2	Ca	Na	K	Mg	Fe	Al	CO_2	H_2S	CH_4	H_2	N_2
	Water phase														Vapour phase				
2	7.52	5.3	22	595	83	54	17.64	501	0.57	434	72	0.008	0.016	0.514	5679.7	224.01	14.830	7.61	69.64
5	7.42	5.6	45	602	55	46	12.84	402	0.7	431	66	0.006	0.019	0.716	4649.6	198.47	1.860	4.92	66.81
10	7.51	8.6	41	795	54	51	12.42	516	1.64	537	96	0.033	0.033	0.554	3298.7	154.6	24.430	2.15	148.86
11	7.50	4.5	17	550	39	51	26.73	472	0.46	393	64	0	0.016	0.553	39.1	26.73	0.020	0.01	0.07
15	7.83	4.6	42	509	54	44	27.21	446	0.43	407	64	0.008	0.016	0.611	2762.4	199	8.090	8.15	90.07
16	7.78	4.1	37	492	71	54	22.99	421	0.29	422	56	0.025	0.008	0.411	4139.0	186.6	6.090	11.79	235.92
19	7.97	3.8	47	326	73	58	37.91	455	0.41	353	45	0.033	0.017	0.756	3081.7	211.22	7.340	8.84	179.35
20	7.61	9.8	15	564	78	65	30.49	533	0.63	418	67	0.034	0.261	0.295	4696.3	330.68	5.640	8.53	37.87
23	7.85	3.1	33	172	79	58	35.94	508	0.7	288	40	0.039	0.031	0.552	4000.6	261.42	2.990	11.9	78.3
26	7.67	1.8	20	252	110	56	34.61	537	0.2	274	42	0.033	0.204	0.760	6846.0	352.74	4.290	10.28	112.54
28	7.68	4.1	68	312	30	33	17.48	408	0.87	288	40	0.007	0.078	0.562	1992.4	177.04	0.980	5.11	60.82
29	7.63	7.3	22	366	34	60	22.84	438	0.54	300	45	0.022	0.043	0.482	2316.2	252.33	1.040	8.84	108.35
30	7.29	2.7	34	362	36	36	13.97	527	0.19	279	49	0.021	0.625	1.098	2842.0	257.38	0.000	0.92	83.84
202	8.31	2.0	60	283	1101	42	6.07	256	0.63	594	102	0.032	0.016	0.687	22522.0	14.94	15.370	0	86.24
301	7.50	4.8	80	171	5078	75	14.5	609	0.47	913	148	0.05	0.014	0.477	301545.0	173.29	21.900	3.48	518.13
302	7.69	2.6	40	373	1148	57	9.01	549	0.8	467	75	0.059	0.015	0.576	62522.0	83.13	27.030	2.89	393.53
304	7.08	3.0	84	47	2763	22	2.63	330	3.15	869	67	1.566	0.127	0.471	564270.0	99.46	30.950	2.13	545.57
306	7.26	5.1	40	203	2102	50	13.3	446	0.97	688	78	0.065	0.073	1.117	246029.0	282.82	81.590	6.1	1189.75
709	8.42	3.4	49	518	196	19	20.65	437	0.95	569	147	0.027	0.014	0.599	3479.0	48.85	6.220	5.33	119.26
714	7.66	2.6	26	498	248	48	31.46	539	0.64	406	79	0.044	0.007	0.766	12686.0	317.62	20.840	9.62	373.28
719	7.58	3.8	66	429	231	36	25.52	464	0.86	423	64	0.032	0.016	1.192	16379.7	297.82	17.650	5.26	286.11
901	8.29	1.9	97	218	464	62	59.89	412	0.56	394	44	0.023	0.023	0.530	10067.8	159.57	6.560	6.05	177.59
902	7.98	1.2	82	174	437	43	4.02	391	1.07	367	34	0.041	0.066	1.736	18428.5	22.61	30.080	0.29	916.84
903	7.69	0.9	86	149	769	38	7.18	370	0.59	412	39	0.033	0.017	1.020	56475.0	76.18	58.360	2.24	2691.69

TABLE 5: Aquifer fluid composition based on a single-phase liquid-only reservoir (Model 1); concentrations are in mg/kg; output from program WATCH (Bjarnason, 2010)

Well	pH	B	SO_4	Cl	CO_2	F	H_2S	SiO_2	Ca	Na	K	Mg	Fe	Al	CO_2	H_2S	CH_4	H_2	N_2
	Water phase														Steam phase				
2	6.60	5.4	22	608	965	55	39.76	512	0.58	444	73	0.008	0.016	0.526	0	0	0	0	0
5	6.47	7.1	58	767	853	58	35.07	513	0.89	549	84	0.008	0.025	0.912	0	0	0	0	0
10	6.72	10.0	47	920	766	59	33.67	597	1.9	622	111	0.039	0.039	0.641	0	0	0	0	0
11	6.67	4.6	17	564	501	52	60.22	484	0.47	403	66	0	0.016	0.567	0	0	0	0	0
15	6.94	4.8	44	535	526	46	42.61	469	0.46	428	68	0.008	0.016	0.643	0	0	0	0	0
16	6.82	4.2	37	497	537	54	30.95	426	0.3	426	57	0.025	0.009	0.416	0	0	0	0	0
19	7.04	3.9	49	334	492	60	48.04	467	0.42	362	46	0.034	0.017	0.775	0	0	0	0	0
20	6.74	11.3	17	652	1004	75	66.55	617	0.73	484	77	0.04	0.302	0.341	0	0	0	0	0
23	6.91	3.3	34	181	752	61	51.19	535	0.74	303	43	0.041	0.033	0.582	0	0	0	0	0
26	6.72	1.8	20	257	1049	56	64.39	546	0.2	279	42	0.033	0.208	0.773	0	0	0	0	0
28	6.78	4.9	83	380	432	40	37.71	497	1.06	351	49	0.008	0.095	0.684	0	0	0	0	0
29	6.72	7.9	23	397	500	66	53.03	475	0.58	325	49	0.023	0.047	0.523	0	0	0	0	0
30	6.46	2.9	37	393	650	39	57.96	573	0.2	303	53	0.022	0.679	1.194	0	0	0	0	0
202	7.32	2.0	60	284	2351	43	5.68	257	0.63	596	103	0.032	0.016	0.690	0	0	0	0	0
301	6.33	4.9	81	174	53017	76	35.93	621	0.48	932	151	0.051	0.015	0.487	0	0	0	0	0
302	6.90	2.6	40	374	4625	57	12.36	551	0.8	469	75	0.059	0.015	0.578	0	0	0	0	0
304	5.56	3.0	85	48	42321	22	8.21	335	3.2	882	68	1.59	0.129	0.478	0	0	0	0	0
306	6.36	5.1	41	204	10334	50	20.97	447	0.97	689	78	0.065	0.073	1.119	0	0	0	0	0
709	6.36	5.1	41	204	10334	50	20.97	447	0.97	689	78	0.065	0.073	1.119	0	0	0	0	0
714	7.71	3.5	51	536	972	19	19.48	452	0.98	589	152	0.028	0.014	0.619	0	0	0	0	0
719	7.04	2.6	26	499	1054	48	46.16	541	0.64	408	79	0.044	0.007	0.769	0	0	0	0	0
901	6.64	3.8	66	432	1541	36	41.06	467	0.86	425	64	0.032	0.016	1.198	0	0	0	0	0
902	6.99	2.0	101	228	1978	65	46.02	431	0.59	413	46	0.024	0.025	0.554	0	0	0	0	0
903	6.69	0.9	86	149	2517	39	8.75	371	0.59	413	39	0.034	0.017	1.022	0	0	0	0	0

The causes for aquifer vapour leading to excess enthalpy of the well discharge at the surface may be two. Heat may be added to the fluid, for example from a hot rock or molten magma, leading to induced boiling at the reservoir temperature. Alternatively, depressurization boiling in the producing aquifer leads to the formation of vapour and water. The vapour phase has a much lower density compared to the liquid water phase and may, therefore, separate depending on the geohydrological conditions of the system. The liquid is assumed to be adsorbed onto mineral grain surfaces, hence being retained in the aquifer. As a result, vapour flows, in excess of water, into the well bore, increasing the vapour-to-water ratio and, hence, the discharge enthalpy. Karingithi et al. (2010) concluded that the cause of excess enthalpy and reservoir vapour was likely caused by phase segregation in the producing aquifer rather than heat addition. This was concluded based on the relationship between the non-volatile concentrations in the discharge fluids. For example, the concentration of Cl in the liquid phase of the well discharge was observed to be relatively constant as a function of discharge enthalpy, whereas the Cl concentration in the total discharge was observed to decrease with increasing enthalpy. Such a trend suggests that phase segregation is the principle process of excess vapour and enthalpy formation (Arnórsson et al., 2007; Scott et al., 2014). The calculated aquifer vapour fraction ranges from an almost liquid-only aquifer (X^{vapour}= ~0) to almost pure vapour (X^{vapour}= ~1), resulting in a discharge enthalpy ranging from ~900 kJ/kg to >2500 kJ/kg.

5. GEOTHERMOMETRY

The aquifer temperatures were calculated based on the reservoir fluid composition for three geothermometers, quartz (t_{qtz}), Na/K ($t_{Na/K}$) and H_2S (t_{H2S}), and those were compared to the measured down-hole temperatures of the producing aquifers. The geothermometer temperatures were both calculated assuming a liquid-only reservoir (Model 1) and two-phase reservoirs (Model 2). The geothermometer temperature functions are listed in Section 2. The results are given in Table 6. In Figure 2 (A & B) and Figure 3, the results are compared to the reservoir temperatures.

The calculated $t_{Na/K}$ for the two models yields the same results. This is to be expected given the temperature is based on the ion ratio of two non-volatiles that are not partitioning between the liquid and vapour phases. Moreover, the measured and calculated Na/K temperatures are in very close agreement, generally within ±10°C.

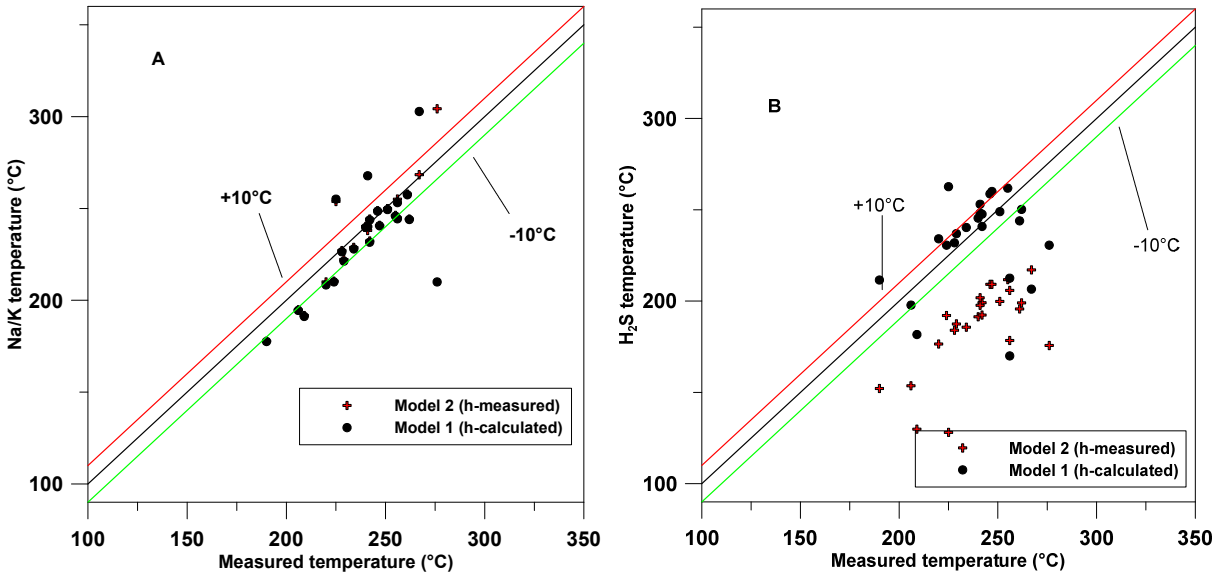

FIGURE 2: (A) $T_{Na/K}$ and (B) T_{H2S} comparison with reservoir temperature

TABLE 6: Geothermometer temperatures (°C) for Olkaria wells

Well	Enthalpy kJ/kg	AquiferT	$t_{NaK}(1)$	$t_{NaK}(2)$	$t_{Qtz}(1)$	$t_{Qtz}(2)$	$t_{H2S}(1)$	$t_{H2S}(2)$
2	1839	251	249	250	266	263	249	200
5	2599	240	240	240	267	234	245	191
10	2531	261	257	258	295	268	244	196
11	1894	246	249	249	258	254	259	209
15	2140	242	244	244	253	247	241	192
16	1534	228	226	227	241	240	232	184
19	1871	229	221	222	253	249	237	187
20	2541	255	246	246	303	273	262	212
23	2191	242	232	232	274	265	248	199
26	1881	247	241	241	277	274	260	209
28	2446	234	228	229	262	236	240	186
29	2158	241	240	240	255	244	253	198
30	2196	225	255	255	286	271	263	206
202	1104	256	253	254	192	191	170	128
301	1653	262	244	244	304	299	250	199
302	1234	256	244	245	279	278	213	178
304	1672	190	178	178	215	214	212	152
306	1037	224	210	210	247	247	231	192
709	1921	276	210	304	247	244	231	176
714	1303	267	303	268	248	275	207	217
719	1259	241	268	238	276	252	248	202
901	1854	220	208	210	242	237	234	177
902	1108	209	191	192	232	231	182	130
903	953	206	194	195	226	225	198	154

Enthalpy = measured enthalpy (kJ/kg); t_{NaK} = sodium potassium geothermometer;
t_{Qtz} = quartz geothermometer; t_{H2S} = hydrogen sulphide geothermometer;
1 = model based on single-phase liquid aquifer.

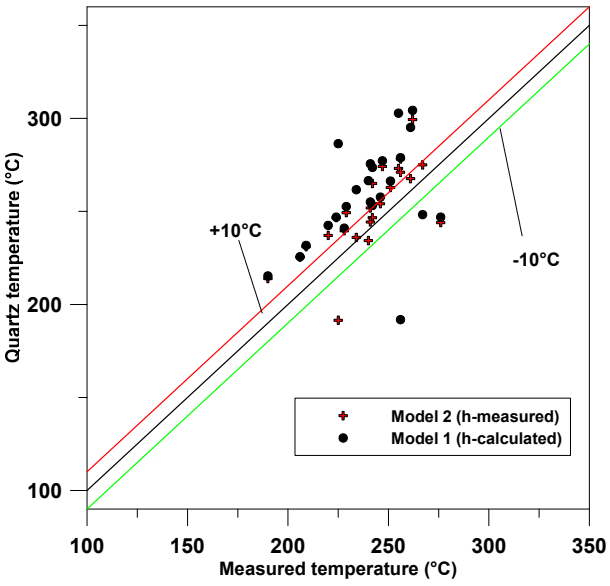

FIGURE 3: T_{qtz} comparison with reservoir temperature

The H_2S temperature for the two models varies considerably. The model based on measured enthalpy has lower H_2S temperature compared to the liquid enthalpy model. This is because in Model 1, a single-phase liquid aquifer was assumed, resulting in higher H_2S concentration in the aquifer fluids and higher temperatures compared to Model 2 which assumed two-phase aquifer fluids. Compared to the measured temperatures, the results of Model 1 are much closer, usually within 10-15°C, whereas the results when assuming two-phase reservoirs were systematically lower than the measured temperatures of >40°C. Karingithi et al. (2010) concluded that the cause of excess enthalpy of the well discharge was caused by phase segregation. This means that the aquifer fluid is close to being a single-phase liquid and then, upon depressurization boiling in the producing aquifer, phase separation occurs. As a result, Model 1, assuming a single-phase liquid reservoir, may be closer to the initial reservoir aquifer conditions; this coincides with the observation of close t_{H2S} and measured temperatures.

The quartz temperatures calculated for the two models show systematically higher values than the measured aquifer temperatures, whereas the results of the two models applied for estimating the aquifer composition are reasonably close. The reason for these discrepancies may be twofold. Firstly, the function used for the calculation of the quartz temperature was based on quartz solubility and may not be entirely correct at >250°C. Alternatively, the reason could be related to too high calculated SiO_2 concentrations in the reservoir, caused by phase segregation that was not taken into account in the aquifer model calculations.

6. FLUID-ROCK INTERACTION

The process of fluid- rock interaction results in the dissolution of the rock and its primary minerals and the formation of alteration minerals. In consideration of fluid-rock interaction, we assume that there is a localised equilibrium between the minerals and the solution. Therefore, temperature and pressure are bound to affect the state of saturation of the different minerals in the system. The Olkaria geothermal system has a liquid-dominated reservoir. Therefore, the enthalpy in the aquifer liquid is usually taken to be that of steam-saturated water at the aquifer temperature. However, some wells have been noted to have excess enthalpy. In the determination of the equilibrium conditions, an important part is the aquifer composition; how it is modelled will determine what state of equilibrium there is. In this analysis, we modelled the impact of the two models on the saturation state of the minerals. Lagat (2004) discussed the hydrothermal minerals that are found within the Olkaria geothermal system. Adularia, albite, biotite, calcite, chlorite, pyrite, epidote, Fe-oxides, fluorite, garnet and illite are the major minerals that have been analysed from drill cuttings. Pyrrhotite, magnetite and wollastonite have not been comprehensively sited but, nevertheless, we discuss their equilibrium with solution in the system. In this study, we discuss the saturation state of andradite, grossular, calcite, clinozoisite, epidote, fluorite, magnetite, prehnite, pyrite, pyrrhotite and wollastonite.

6.1 Calcite, fluorite and wollastonite

The calcite saturation in the aquifer fluid of the selected Olkaria wells is shown in Figure 4A and is based on mineral solubility equations in Tables 2 and 3. The values for the calcite activity product generally plot around the equilibrium constant or closely approach the equilibrium constant line for the majority of the samples. However, there are some parts that indicate a deviation from the equilibrium constant at both under-saturation and over-saturation. The saturation index based on the calculated enthalpy model, i.e. assuming the aquifer enthalpy to be that of steam-saturated water at aquifer temperature, has most of the values indicating under-saturation of calcite in the aquifer. Most of the wells plot below the equilibrium curve with around -2 SI units, while wells 202 and 302 from the Olkaria Central and West sectors are over-saturated. The wells in this part of the field have very high dissolved CO_2 to the order of > 1000 ppm, considered high for the Olkaria system, and pH in the range of 9. The second model based on the measured enthalpy, i.e. the measured enthalpy of the discharge being higher than that in the aquifer, indicates equilibrium although some samples were super-saturated with respect to calcite. Some samples were under-saturated but this seems to be a systematic error. In this model, the wells in the East part of the field are in equilibrium or approaching equilibrium. This equilibrium will shift depending on the boiling process and the precipitation of calcite, as seen from the two models and the CO_2 and pH values applied in the modelling of the equilibrium.

The fluorite saturation state is shown in Figure 4B. The system is under-saturated with respect to fluorite for most of the field. This under-saturation is consistent for both models and is up to as high as 2.5 SI units. Some wells in the East sector of the field indicate an approach to equilibrium or slight super-saturation. The depicted super-saturation is consistent for both models although it is minor to magnitudes of 0.5 SI units. This super-saturation is centred in wells 20, 29, 23 and 20 which are in a zone of heating

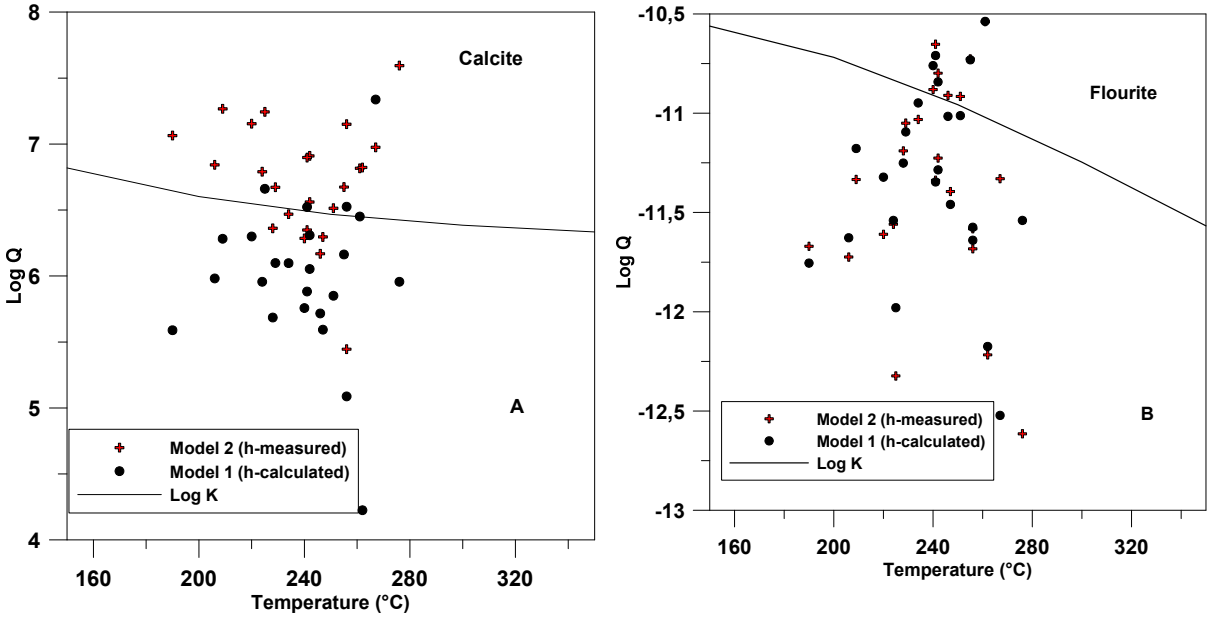

FIGURE 4: Saturation state of aquifer water with respect to (A) calcite and (B) fluorite

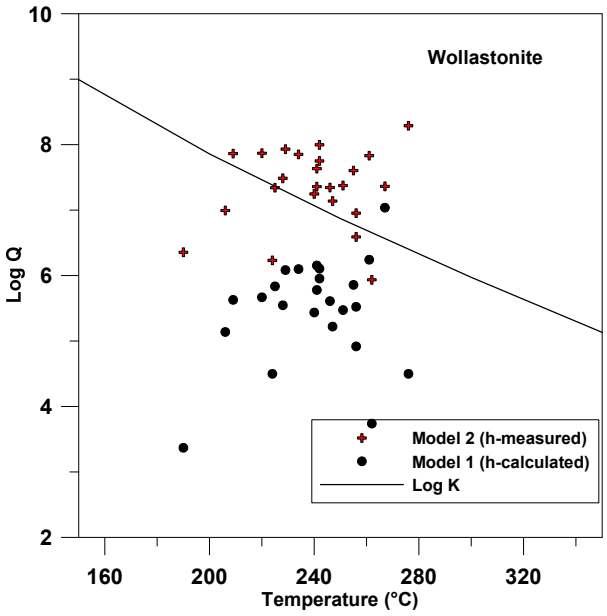

FIGURE 5: Saturation state of aquifer water with respect to wollastonite

up-flow in the Olkaria system. Fluorite generally shows retrograde solubility and will be affected by depletion of Ca^{+2} in the solution.

The saturation state of wollastonite is presented in Figure 5. It is seen that a clear pattern emerges where the two models give distinctively different saturation states for wollastonite. The activity product of the mineral, based on the measured enthalpy model, shows a definite super-saturation of wollastonite, although there are some scattered samples it is close to equilibrium. These are probably a systematic error. The activity products obtained from the model, based on calculated enthalpy, indicate an overall under-saturation of wollastonite in the system. The saturation state of wollastonite is based on the activity of Ca^{+2}. Thus, the values for the activity of Ca^{+2} in the two models differ, hence the difference in the observed saturation state for wollastonite in the Olkaria system.

6.2 Magnetite, pyrite and pyrrhotite

The saturation state of pyrite, pyrrhotite and magnetite is shown in Figures 6 and 7, respectively. Magnetite was observed to be super-saturated in almost all cases, independent of the assumptions made for calculating the aquifer fluid composition. There is a scatter of the SI values, ranging from -27 to -22 SI units. On the other hand, the waters were observed to be under-saturated with respect to both pyrite and pyrrhotite, by up to 2 and 4 SI units, respectively.

Pyrite has been observed as an alteration mineral in the Olkaria system, whereas magnetite and pyrrhotite are not (Lagat, 2004). Magnetite super-saturation implies that it may, however, form, whereas

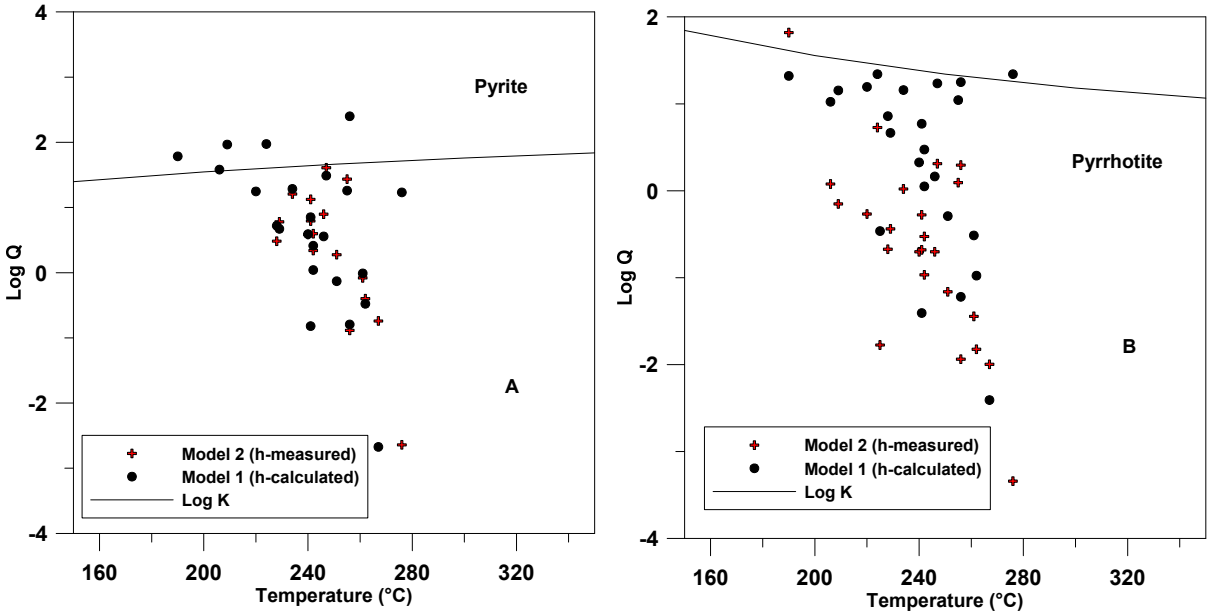

FIGURE 6: Saturation state of aquifer water with respect to (A) pyrite and (B) pyrrhotite

pyrite and pyrrhotite under-saturation suggests that these minerals are unstable and not forming; this is somewhat conflicting with the observed mineralogy at Olkaria. The discrepancies may be related to difficulties in computing the activities of iron containing aqueous species. Firstly, iron is found in two oxidation states, $Fe^{II}$and Fe^{III}; magnetite contains both, whereas pyrite and pyrrhotite only containing Fe^{II}. In geothermal fluids, both oxidations may exist, depending on temperature and pH (Gunnlaugsson and Arnórsson, 1982). In order to calculate the equilibrium of Fe aqueous speciation, a redox couple needs to be selected, this being the H_2S/SO_4 couple in WATCH. As pointed out by Stefánsson and Arnórsson (2002), overall redox equilibrium may not exist, making the estimation of the ration of Fe^{II}/Fe^{III} from the H_2S/SO_4 ratio questionable. Also, as pointed out by Arnórsson et al. (2002), the thermodynamic equilibrium constants for Fe^{II} and Fe^{III} under hydrothermal conditions are somewhat uncertain, resulting in large uncertainties in the calculated Fe^{II}/Fe^{III} ratio and the Fe^{II} and Fe^{III} aqueous speciation.

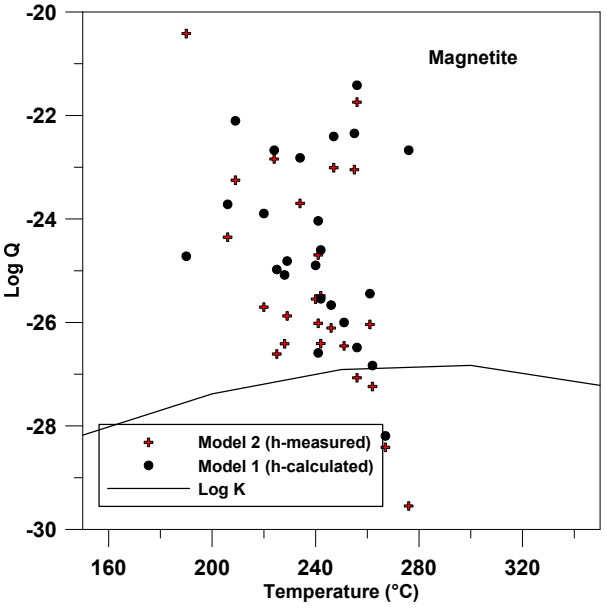

FIGURE 7: Saturation state of aquifer water with respect to magnetite

6.3 Andradite-grossular, clinozoisite-epidote and prehnite

Andradite and grossular are end members of the garnet solid solution. Grossular has the formula $Ca_2Al_2Si_4O_3$ where the Al can be replaced by Ferric ion, while the Ca is partially replaced by ferrous ion. The andradite end member is represented by $Ca_2Fe_2Si_3O_{12}$. The activity product of andradite from Figure 8A indicates a general super-saturation of andradite in the Olkaria system, as analysed for both models. Four samples show equilibrium, but this are suspected to be a result of a systematic error. The saturation state of andradite, based on the second model however, has a smaller deviation from equilibrium of about 2.0 SI units.

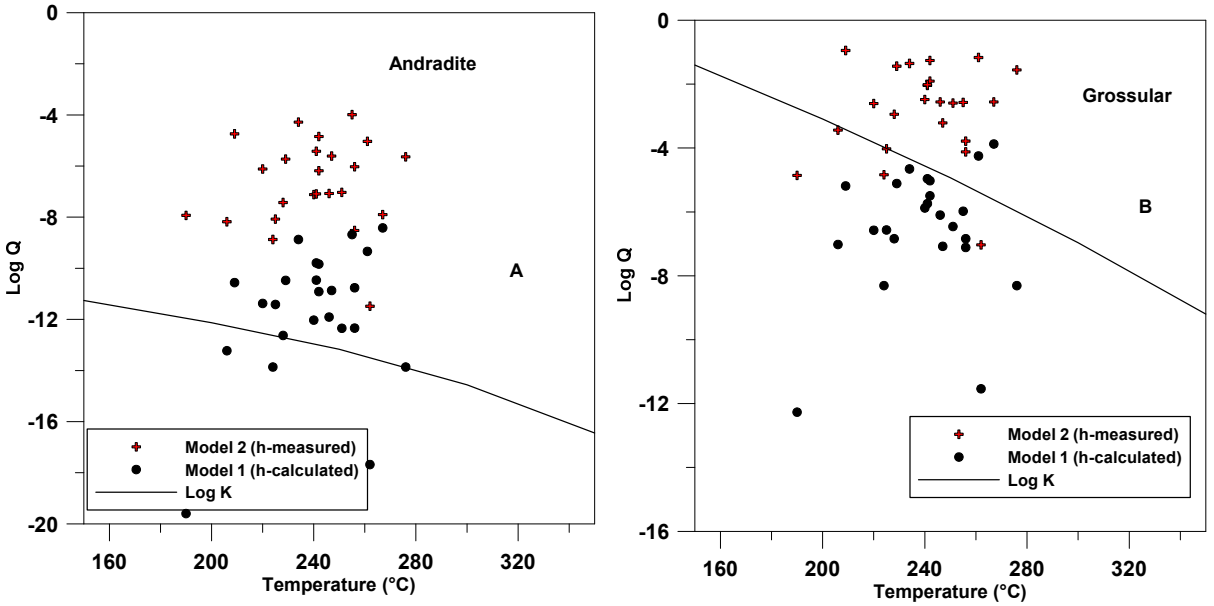

FIGURE 8: Saturation state of aquifer water with respect to (A) andradite and (B) grossular

Figure 8B indicates the activity product of the mineral grossular. The two models used indicate different saturation states for grossular. The model based on measured enthalpy indicates super-saturation of grossular in solution for the whole Olkaria system. The model based on calculated enthalpy indicates under-saturation of grossular for the Olkaria system.

Epidote is a common mineral in the Olkaria system and is used as an indicator mineral for high temperature zones within the Olkaria reservoir. The epidote in Olkaria has the composition $Ca_2FeAl_2Si_3O_{12}$ (OH). The activity product of epidote from Figure 9B indicates that, overall, the aquifer water in the Olkaria system is epidote super-saturated, based on both the models. Clinozoisite forms a continuous solid solution series with epidote and is obtained by substitution of Fe^{+3} in the Al site. The model based on the calculated enthalpy shows that the aquifer water in Olkaria closely approaches equilibrium, as the activity products are scattered around the equilibrium constant curve. However, the wells, located in Olkaria West and Olkaria Central, show a slight under-saturation with respect to clinozoisite, based on this model. The second model, based on measured enthalpy, indicates super-

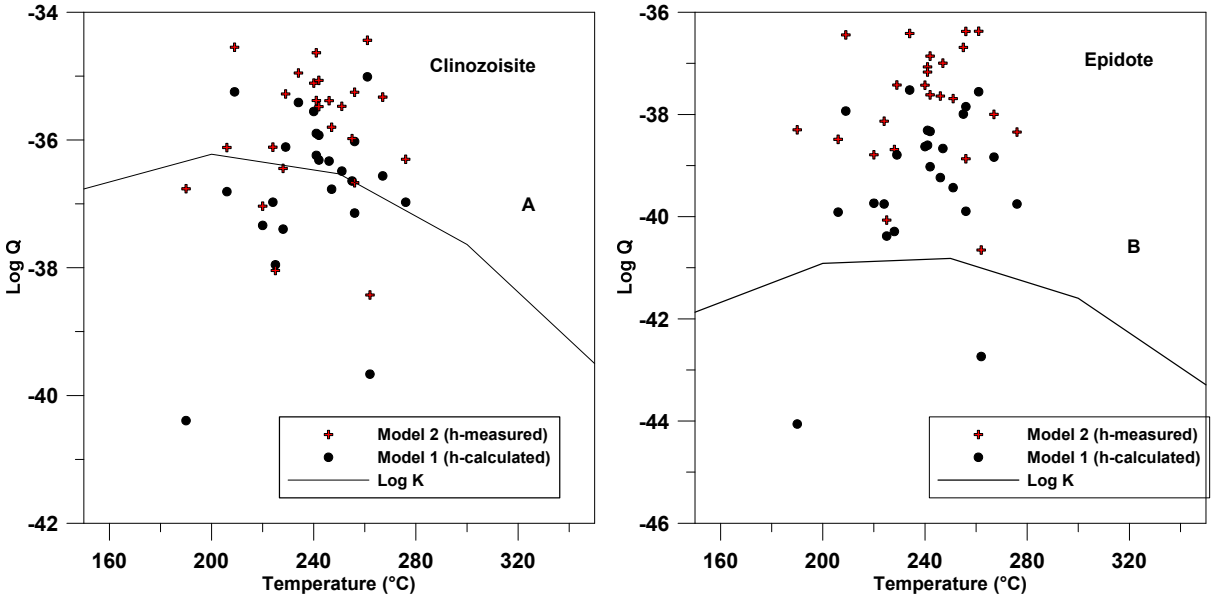

FIGURE 9: Saturation state of aquifer water with respect to (A) clinozoisite and (B) epidote

saturation of clinozoisite in the aquifer water. The wells in Olkaria West and Olkaria Central closely approach equilibrium for this model. Some samples, however, show under-saturation, possibly the result of a systematic error. The composition of epidote in the Olkaria system lies between the clinozoisite and epidote end-member composition, possibly resulting from the observed saturation with respect to the end-member mineral composition (Karingithi et al., 2010). Moreover, the aqueous speciation of iron is somewhat uncertain and $Fe(OH)_4^-$ aqueous activity may be possibly over-estimated, resulting in super-saturation of Fe^{III}-bearing minerals like epidote and magnetite.

Prehnite is expressed by the chemical formula $Ca_2Al(AlSi_3O_{10})(OH)_2$ where Fe^{3+} could substitute for Al in the structure. Prehnite has a variable saturation state, based on the two models. The model based on calculated enthalpy shows that the activity product of prehnite scatters around the equilibrium constant curve (Figure 10). Super-saturation is very minimal around the Olkaria system, based on this model. The activity product based on the measured enthalpy model shows a systematic super-saturation with respect to prehnite for the aquifer water in Olkaria. Three samples deviate from this, but could possibly be errors.

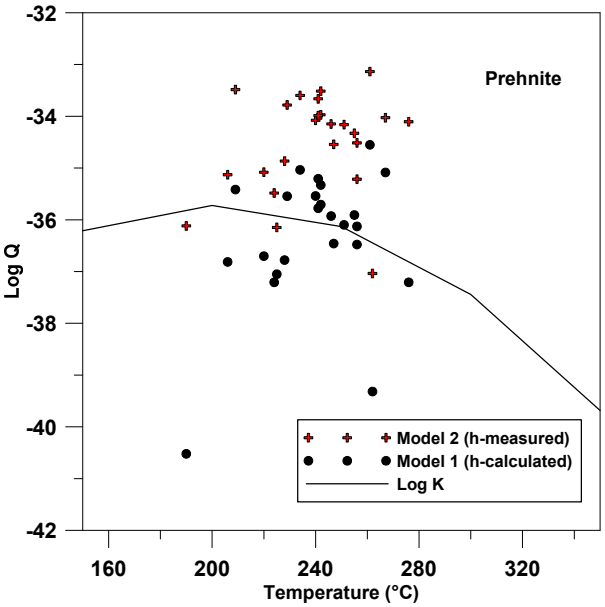

FIGURE 10: Saturation state of aquifer water with respect to prehnite

6.4 Gas equilibria

Concentrations of reactive gases can be controlled by equilibrium with respect to specific mineral assemblages. Various mineral assemblages have been expressed that can control this reaction, as seen in Table 3. Figure 11A shows the state of equilibrium between H_2 and four mineral assemblages, based on the two models. The model based on measured enthalpy shows a complete departure from

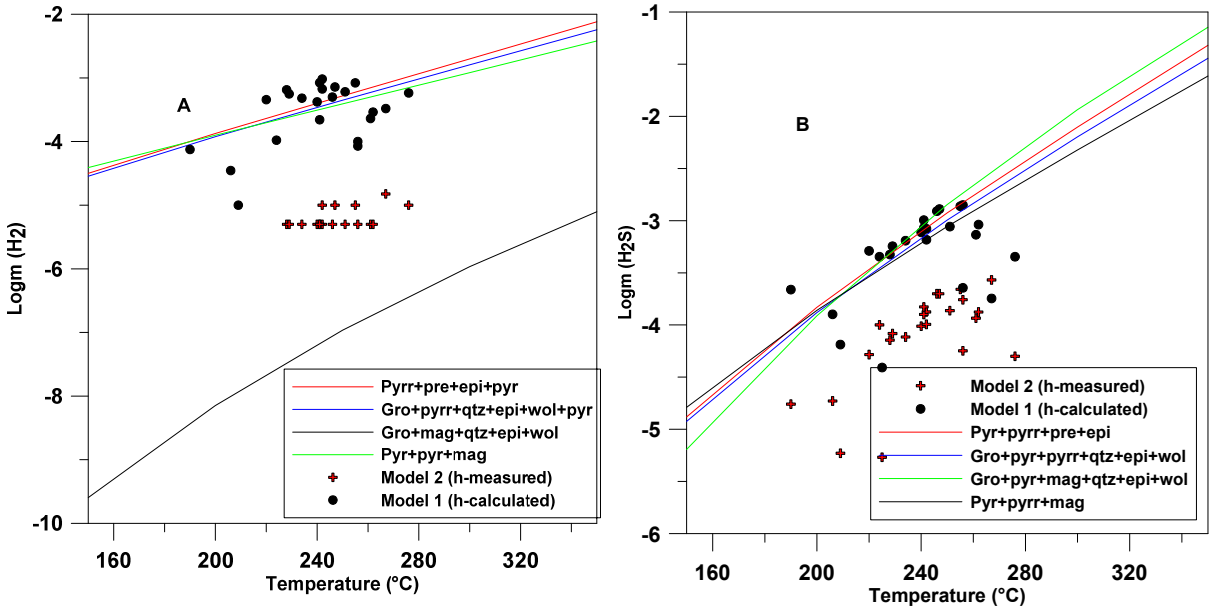

FIGURE 11: State of equilibrium between (A) dissolved H_2; and (B) H_2S in the aquifer water and mineral buffers

equilibrium with all the mineral assemblages. On the other hand, the model assuming a liquid-only aquifer shows close to equilibrium with respect to H_2. What controlling mineral buffer reactions are involved is hard to assess as many show very close equilibrium H_2 concentrations.

Figure 11B shows the state of equilibrium between H_2S and four different mineral assemblages. The H_2S concentrations, based on the measured enthalpy, show a considerable departure from equilibrium with all the four mineral assemblages, whereas those calculated assuming a liquid-only aquifer are very close to equilibrium with respect to several mineral buffer reactions. As with H_2, it is very difficult to assess exactly which minerals are involved.

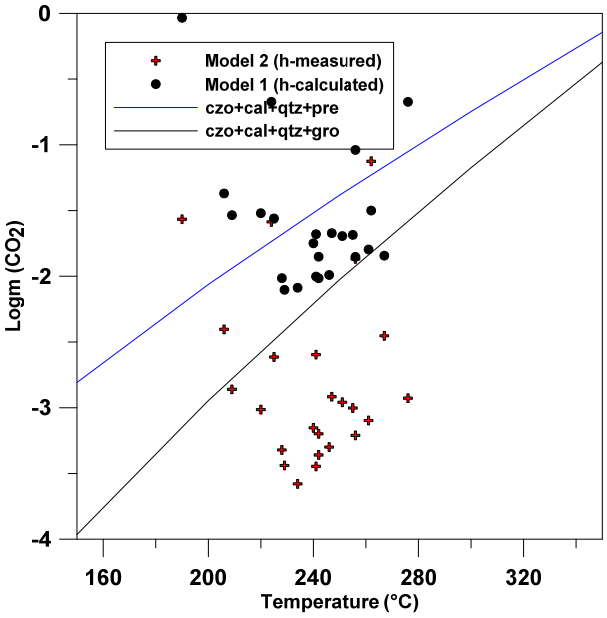

FIGURE 12: State of equilibrium between dissolved CO_2 in the aquifer water and mineral buffers

Figure 12 illustrates the state of equilibrium of CO_2 concentrations in Olkaria aquifer waters with two mineral assemblages. The concentrations based on the measured enthalpy are below equilibrium with the mineral assemblage. On the other hand, for Model 1 assuming a liquid-only reservoir, closer to equilibrium conditions are observed between the proposed mineral buffer reactions and the calculated aquifer CO_2 concentrations. The fluids in the Olkaria East and Northeast closely approach equilibrium with the mineral assemblage clinozoisite-calcite-quartz-grossular, whereas the fluids in the Dome sector have concentrations that closely approach equilibrium with the mineral assemblage clinozoisite-calcite-quartz-prehnite. However, bearing in mind all the uncertainties associated with the calculation of the aquifer fluid composition and its relationship with the exact equilibrium CO_2 concentration with respect to the mineral buffer reactions, it is very difficult to assess with confidence which minerals are truly involved in buffering the concentration of CO_2 in the aquifers of the Olkaria geothermal system.

7. SUMMARY AND CONCLUSIONS

The fluid composition and mineral-fluid interaction in the Olkaria geothermal system were studied. Fluid-rock interaction is one of the key reactions of interest in geothermal systems. There is a close approach to equilibrium between common geothermal minerals and the fluids within the reservoir, controlling the composition of most major elements in the fluid. The assessment of fluid-rock equilibria from the fluid composition of surface well discharges largely relies on the assumptions made when calculating the subsurface aquifer fluid composition. Two models were applied in the evaluation of aquifer fluid composition. Model 1 is based on a calculated enthalpy and considers a single-phase liquid-only reservoir. Model 2 considers a two-phase liquid and vapour reservoir and uses the measured enthalpy. The concentrations of non-volatile elements for the two models are similar, except for the discharge fluids that approach that of pure steam. Yet, the concentrations of non-volatiles in the liquid phase of two-phase reservoirs are somewhat lower in most cases. There is a marked difference between the two models in the case of the volatiles. The reason for this is the volatiles portioning into the vapour phase, some completely upon initial boiling like H_2 and CH_4, whereas others are distributed between the two phases like CO_2 and H_2S. As a result, the aqueous concentrations of the non-volatiles are low when assuming two-phase reservoirs, compared to single-phase liquid reservoirs. The model based on measured enthalpy has lower H_2S temperature compared to the liquid enthalpy model. This is because,

in Model 1, a single-phase liquid aquifer was assumed, resulting in higher H_2S concentrations in the aquifer fluids and higher temperatures compared to Model 2, which assumed two-phase aquifer fluids. The initial aquifer was taken to be a single-phase liquid that was undergoing phase separation. As a result, Model 1 which assumes a single-phase liquid reservoir may be closer to the initial reservoir aquifer conditions, as it coincides with the measured temperatures. The Ca-Al minerals show varying equilibrium, based on the model used. The measured enthalpy evaluations show a general super-saturation of the minerals grossular, andradite, clinozoisite, epidote and prehnite in the Olkaria aquifer water. The aquifer water, based on this system, is degassed relative to equilibrium and, thus, there is lower non-volatile concentration in the water. The liquid enthalpy values show that the Ca-Al minerals closely approach equilibrium with the aquifer water. A simultaneous equilibrium between clinozoisite, prehnite, quartz and the solution then fixes the activity of the Ca^{+2}. The Fe^{II} minerals pyrite and pyrrhotite are under-saturated in the Olkaria aquifer water, based on the two models, while magnetite is super-saturated. This is a discrepancy, given that pyrite is found in the Olkaria system. The thermodynamic equilibrium constants for Fe^{II} and Fe^{III} under hydrothermal conditions are somewhat uncertain, resulting in large uncertainties in the calculated Fe^{II}/Fe^{III}ratio and the Fe^{II} and Fe^{III} aqueous speciation. Moreover, the aqueous speciation of iron is somewhat uncertain, and $Fe(OH)_4^-$ aqueous activity may possibly be over-estimated, resulting in super-saturation of Fe^{III}-bearing minerals like epidote and magnetite. The H_2 and H_2S concentrations in the aquifer water of the single-phase liquid reservoir are closely controlled by equilibrium with specific mineral assemblages. Which controlling mineral buffer reactions are involved is hard to assess, as many show very close equilibrium to these concentrations. With uncertainties associated with the calculation of the aquifer fluid composition and the relationship to the exact equilibrium CO_2 concentration with respect to the mineral buffer reactions, it is very difficult to assess with confidence which minerals are truly involved in buffering the concentration of CO_2 in the aquifer Olkaria geothermal system.

ACKNOWLEDGEMENTS

I would like to express my sincere appreciation to Mr. Lúdvík S. Georgsson, Director of UNU-GTP, for the opportunity to participate in the Geothermal Training Programme in 2014. I would also like to thank the UNU staff: Mr. Ingimar G. Haraldsson, Ms María S. Gudjónsdóttir, Ms Málfrídur Ómarsdóttir, Ms Thórhildur Ísberg and Mr. Markús A.G. Wilde, for their assistance and support during my stay in Iceland. I would also like to thank my supervisor, Prof. Andri Stefánsson, for his guidance, support and sharing of valuable knowledge in the course of my project. I would also wish to thank Mr. Thráinn Fridriksson for his support and advice. My appreciation also goes to the Kenya Electricity Generating Company for granting me leave to attend this training. Finally, my gratitude goes to my family, friends and UNU-GTP 2014 fellows for their support.

REFERENCES

Ambusso, W.J., and Ouma, P.A., 1991: Thermodynamic and permeability structure of Olkaria North-east geothermal field: Olkaria fault. *Geothermal Resources Council, Transactions, 15,* 237-242.

Ármansson, H., and Ólafsson, M., 2000: *Collection of geothermal fluids for chemical analysis*. ÍSOR – Iceland GeoSurvey, Reykjavík, report ISOR-2006/101, 17 pp.

Arnórsson, S., and D'Amore, F., 2000: Monitoring of reservoir response to production. In: Arnórsson, S. (ed.), *Isotopic and chemical techniques in geothermal exploration, development and use. Sampling methods, data handling, and interpretation*. International Atomic Energy Agency, Vienna, 306-341.

Arnórsson, S., and Stefánsson, A., 1999: Assessment of feldspar solubility constants in water in the range 0-350°C at P_{sat}. *Am. J. Sci., 299,* 173-209.

Arnórsson, S., Gunnlaugsson, E., and Svavarsson, H., 1983: The chemistry of geothermal waters in Iceland. II. Mineral equilibria and independent variables controlling water compositions. *Geochim. Cosmochim. Acta*, *47*, 547-566.

Arnórsson, S., Sigurdsson, S. and Svavarsson, H., 1982: The chemistry of geothermal waters in Iceland I. Calculation of aqueous speciation from 0°C to 370°C. *Geochim. Cosmochim. Acta, 46,* 1513-1532.

Arnórsson, S., Stefánsson, A., and Bjarnason, J.Ö., 2007: Fluid-fluid interaction in geothermal systems. *Reviews in Mineralogy & Geochemistry, 65,* 229-312.

Arnórsson, S., Bjarnason, J.Ö., Giroud, N., Gunnarsson, I., and Stefánsson, A., 2006: Sampling and anaylsis of geothermal fluids, *Geofluids, 6,* 203-216.

Arnórsson, S., Gunnarsson, I., Stefánsson, A., Andrésdóttir, A., and Sveinbjörnsdóttir, A.E., 2002: Major element chemistry of surface- and ground waters in basaltic terrain, N-Iceland. I. Primary mineral saturation. *Geochim. Cosmochim. Acta, 66,* 4015-4046.

Bjarnason, J.Ö., 2010. *The speciation program WATCH* (vers. 2.4). ISOR – Iceland GeoSurvey, Reykjavík.

Clarke, M.C.G., Woodhall, D.G., Allen, D., and Darling G., 1990: *Geological, volcanological and hydrogeological controls on the occurrence of geothermal activity in the area surrounding Lake Naivasha, Kenya, with coloured 1:100 000 geological maps.* Ministry of Energy, Nairobi, 138 pp.

Giggenbach, W.F., 1981: Geothermal mineral equilibria. *Geochim. Cosmochim. Acta, 45*, 393-410.

Gunnarsson, I. and Arnórsson S., 2000: Amorphous silica solubility and the thermodynamic properties of $H_4SiO_4°$ in the range of 0° to 350°C at P_{sat}. *Geochim. Cosmochim. Acta, 64*, 2295-2307.

Gunnlaugsson, E., and Arnórsson, S., 1982: The chemistry of iron in geothermal systems in Iceland. *J.Volcanol. & Geotherm.Res. 14*, 281-299.

Kandie, R., Mwania, M. and Rono, I., 2014: *An update of the geological conceptual model of the greater Olkaria Geothermal field*. KenGen - Kenya Electricity Generating Company Ltd., internal report.

Karingithi, C.W., Arnórsson, S., and Grönvold, K., 2010: Processes controlling aquifer fluid compositions in the Olkaria geothermal system, Kenya. *J. Volcanol.& Geotherm. Res., 196-3/4,* 57-76.

Lagat, J.K., 2004: *Geology, hydrothermal alteration and fluid inclusion studies of the Olkaria Domes geothermal field, Kenya.* University of Iceland, MSc thesis, UNU-GTP, Iceland, report 2, 71 pp.

Naylor, W.I., 1972: *Geology of the Eburru and Olkaria prospects.* U.N. Geothermal Exploration Project, report.

Odongo, M.E.O., 1984: *Geology of the Olkaria volcanic complex.* KPC, Kenya, internal report GL/OW/20.

Scott, S., Gunnarsson, I., Arnórsson, S. and Stefánsson, A., 2014: Gas chemistry, boiling and phase segregation in a geothermal system, Hellisheidi, Iceland. *Geochimica et Cosmochimica Acta, 124,* 170-189.

Stefánsson, A., and Arnórsson, S., 2002: Gas pressures and redox reactions in geothermal fluids in Iceland. *Chemical Geology, 190,* 251-271.

Strecker, M.R, Blisniuk, P.M., and Eisbacher, G.H., 1990: *Rotation of extension direction in the Central Kenya Rift.Geology, 18*, 299-302.

Wambugu, J.M., 1995: *Geochemical update of Olkaria West geothermal field.* Kenya Power Company, Ltd., internal report, 40 pp.